AGU PUBLICATIONS

JGR

Journal of Geophysical Research: Solid Earth

RESEARCH ARTICLE
10.1002/2016JB013469

Key Points:
- Explicit incorporation of material heterogeneity induced from grain size variation
- Influence of grain size heterogeneity on strength and deformation behavior
- Influence of grain size heterogeneity on microcracking process

Correspondence to:
L. N. Y. Wong,
lnywong@hku.hk

Citation:
Peng, J., L. N. Y. Wong, and C. I. Teh (2017), Influence of grain size heterogeneity on strength and microcracking behavior of crystalline rocks, *J. Geophys. Res. Solid Earth*, *122*, 1054–1073, doi:10.1002/2016JB013469.

Received 17 AUG 2016
Accepted 5 FEB 2017
Accepted article online 7 FEB 2017
Published online 24 FEB 2017

Influence of grain size heterogeneity on strength and microcracking behavior of crystalline rocks

Jun Peng[1,2], Louis Ngai Yuen Wong[3], and Cee Ing Teh[2]

[1]State Key Laboratory of Water Resources and Hydropower Engineering Science, Wuhan University, Wuhan, China, [2]School of Civil and Environmental Engineering, Nanyang Technological University, Singapore, [3]Department of Earth Sciences, University of Hong Kong, Hong Kong

Abstract This study numerically investigates the influence of material heterogeneity on the strength and deformation behavior and the associated microcracking process of a felsic crystalline rock using a grain-based modeling approach in two-dimensional Particle Flow Code. By using a heterogeneity index defined in this study, the heterogeneity induced by variation of grain size distribution can be explicitly incorporated into the numerical specimen models quantitatively. Under compressive loading, the peak strength and the elastic modulus are found to increase as the numerical model gradually changes from heterogeneous to homogeneous, i.e., a decrease of heterogeneity index. Meanwhile, the number of grain boundary tensile cracks gradually decreases and the number of intragrain cracks increases at the moment of failure. However, the total number of generated microcracks seems not to be significantly influenced by heterogeneity. The orientation of grain boundary microcracks is mainly controlled by the geometry of assembled grain structure of the numerical specimen model, while the orientation of intragrain microcracks is to a large degree influenced by the confinement. In addition, the development of intragrain cracks (both tensile and shear) is much more favored in quartz than in other minerals. Under direct tensile loading, heterogeneity is found to have no significant influence on the simulated stress-strain responses and rock strength. Only grain boundary tensile cracks are generated when the numerical models are loaded in direct tension, and the position of generated macroscopic fracture developed upon failure of the specimen is largely affected by heterogeneity.

1. Introduction

Rock is typically a heterogeneous material composed of different types of inherent microstructures. The microstructures of a rock at the grain scale are usually associated with different mineral aggregations and microdefects such as microcracks, voids, and cleavage planes [*Duan and Kwok*, 2016; *Hallbauer et al*., 1973; *Kranz*, 1983; *Olsson and Peng*, 1976]. Numerous laboratory test results indicate that the strength and deformation responses and the associated microcracking behavior of rocks are to a large extent affected by the internal microstructures [*Brace et al*., 1966; *Eberhardt et al*., 1998; *Fredrich et al*., 1990; *Martin and Chandler*, 1994; *Wong*, 1982a; *Zhao et al*., 2014].

The aggregation of internal microstructures introduces the material heterogeneity of the rock. One key effect of material heterogeneity is the creation of local tensile stress concentration even when the rock is subjected only to compressive loading [*Blair and Cook*, 1998a; 1998b; *Gallagher et al*., 1974]. Previous studies reveal that the primary mechanism of crack initiation, propagation, and coalescence is due to local tensile cracking. The shear cracking becomes dominant when sufficient tensile damage has been generated or the applied confining pressure is sufficiently high [*Brace et al*., 1966; *Diederichs*, 2003; *Martin and Chandler*, 1994; *Tapponnier and Brace*, 1976]. Therefore, the material heterogeneity is an important factor that needs to be considered when studying the microcracking behavior of rocks. The heterogeneity effect on the microcracking behavior of rocks, however, is difficult to be studied in laboratory testing because the rock specimen must be destroyed if the internal heterogeneity is to be observed and characterized. Although X-ray computerized tomography can successfully differentiate the microdefect phase and mineral phase without destroying the specimen, the different constituent minerals are difficult to be distinguished [*Geraud et al*., 1998; *Peng et al*., 2015; *Ren and Ge*, 2004; *Sufian and Russell*, 2013]. Alternatively, numerical methods have had some prospects of success in recent years to investigate the heterogeneity effect on the cracking processes of rocks.

In general, two approaches are available for incorporating material heterogeneity into numerical models. In the first approach, which is known as the implicit approach, the material heterogeneity is implicitly

incorporated via a stochastic distribution of rock properties. For example, a Weibull distribution is used to account for the failure strength and elastic modulus of elements which are randomly distributed throughout the specimen [*Tang et al*., 2000]. The heterogeneity effect on the mechanical behavior of rocks under compressive loading is studied using this method [*Liu et al*., 2004; *Wong et al*., 2006]. Lattice models have also been utilized to incorporate the material heterogeneity by changing the strength and size of the lattice elements [*Blair and Cook*, 1998a, 1998b; *Schlangen and Garboczi*, 1997; *Schlangen and van Mier*, 1992]. These implicit modeling methods have demonstrated that heterogeneity has a great influence on the mechanical behavior of rocks. However, the choice of input properties is to some extent subjective and highly dependent on the parameters in the statistical distribution.

In the second approach, which is known as the explicit approach, the heterogeneity is explicitly described in the numerical specimen model to be simulated. For instance, the mineral grains inside the rock specimen were explicitly reproduced using a Voronoi tessellation technique which was implemented into Universal Distinct Element Code (UDEC) [*Lan et al*., 2010]. It was found that the grain scale geometric and elastic heterogeneity had a significant influence on the microcracking behavior and macroscopic response of brittle rocks under uniaxial compression tests. By using this methodology, the crack initiation stress was also found to be extensively affected by material heterogeneity [*Mohsen and Martin*, 2014]. Similarly, *Potyondy* [2010] developed a grain-based modeling approach in two-dimensional Particle Flow Code (PFC2D) to mimic the grain-based material such as crystalline rocks. The numerical specimen was generated by matching the grain size distribution and mineral content which was obtained from laboratory characterization. The above two methods are based on the principles of discrete element method. The combined finite-discrete element method was also proposed to incorporate the microscale heterogeneity explicitly to accurately capture the mechanical behavior of rocks [*Mahabadi et al*., 2012]. The microcracking behavior of a rock specimen in Brazilian tensile test was found to be influenced by the microscale heterogeneity and microscopic defects [*Mahabadi et al*., 2014]. More recently, *Manouchehrian and Cai* [2016] introduced the material heterogeneity into an Abaqus model which is an explicit finite element method using Python scripts. Their simulation results indicated that heterogeneity had a significant effect on the intensity of unstable rock failure in unconfined and confined compression tests.

In our recent study, the grain-based modeling approach in PFC2D was demonstrated to be promising for studying the microcracking behavior of crystalline granitic rocks [*Wong and Maruvanchery*, 2016]. The grain-based model in PFC2D could not only simulate the microcrack initiation and interaction at the grain boundary but also capture the microcracking events inside the constituent grains. That previously calibrated model is used in this study to further investigate the influence of material heterogeneity on the strength and microcracking behavior of a crystalline rock. By defining a heterogeneity index, the heterogeneity induced by variation of grain size distribution is explicitly incorporated into the numerical specimens quantitatively. The rock strength and deformation behavior and the associated microcracking process of numerical models with different heterogeneity indices are then examined and discussed.

2. Methodology

2.1. Grain-Based Modeling Approach in PFC2D

The grain-based modeling approach in PFC2D which was proposed by *Potyondy* [2010] is used in this study to investigate the material heterogeneity effect on rock strength and microcracking behavior. The microproperties in a real rock, such as grain size distribution and mineralogical composition, can be reflected in the grain-based model. As illustrated in Figure 1, during the initial disc packing stage, the grain size distribution and mineralogical composition are assigned with parameters which are determined from the thin section examination of a rock specimen. The PFC2D grain-based modeling approach generates polygonal grain structure which is representative of the crystalline rocks. The numerical specimen is generated by overlaying the grain structure with a number of smaller discs filling the grains. The discs inside the grains are bonded by parallel bonds, and the discs along the grain interfaces are assigned with the smooth-joint contacts.

As shown in Figure 2a, in PFC2D, a parallel bond can be envisioned as a set of elastic springs, uniformly distributed over a rectangular cross section lying on the contact plane and centered at the contact point between two particles. The smooth-joint contact simulates the behavior of an interface regardless of the local particle contact orientation along the interface (see Figure 2b). The strength of parallel bond and smooth-

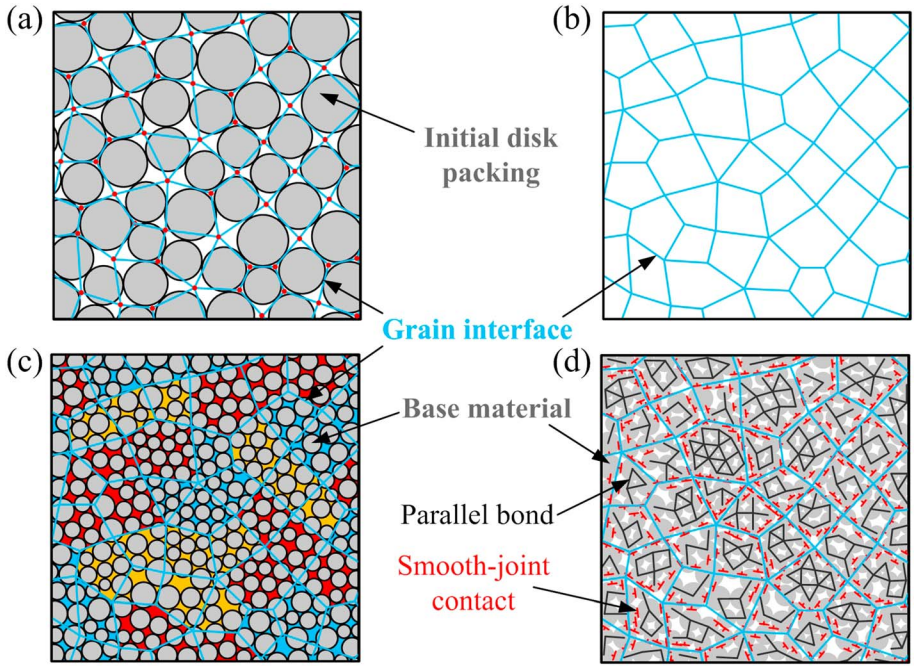

Figure 1. Generation of grain-based model in PFC2D. (a) Initial particle packing. (b) Polygonal grain structure (blue lines) (the initial particles are deleted). (c) Bonded particle model overlaid on the grain structure (three grain types are identified with different colors). (d) Grain-based model consisting of discs bonded together with parallel bonds (black) inside the grains and smooth-joint contacts (red) along the interfaces between the grains (reproduced from *Potyondy* [2010] and *Bahrani et al.* [2014]).

joint contact is defined by the tensile strength, cohesion, and friction angle. When a parallel bond breaks (either in shear or tension), the residual strength is controlled by the friction coefficient of the discs in contact and the disc size, which generates a local dilation and causes the discs to move around each other. However, when a smooth-joint contact breaks (either in tension or shear), its residual strength is defined by the smooth-joint friction coefficient. The discs that are located on opposite sides of a smooth-joint plane can overlap to allow particle sliding along the joint plane (with no local geometric dilation) rather than forcing the discs to move around one another.

The procedure of generating a grain-based model in PFC2D is not presented here. Interested readers can refer to *Potyondy* [2010] or *Bahrani et al.* [2014] for more details. One merit of the PFC2D grain-based model

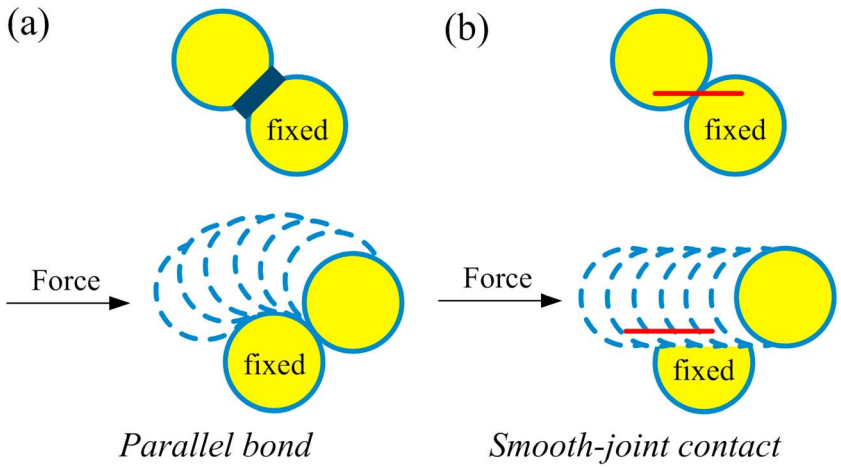

Figure 2. Illustration of disc movements after breakage of (a) parallel bond and (b) smooth-joint contact [after *Bahrani et al.*, 2014].

Table 1. Parameters for the Generated Numerical Grain-Based Models

Specimen No.	Average Grain Size, R_a (mm)	Heterogeneity Index, H	Mean Grain Size of Minerals r_i (mm)			
			K-Feldspar	Quartz	Plagioclase	Biotite
HE1	2.1	1.12	3.0	1.5	3.5	0.5
HE2	1.9	1.02	2.5	1.5	3.0	0.5
HE3	2.0	0.79	2.5	1.5	3.0	1.0
HE4	1.9	0.69	2.5	1.5	2.5	1.0
HE5	2.0	0.35	2.0	2.0	2.5	1.5
HE6	2.0	0	2.0	2.0	2.0	2.0

is that the model can not only simulate the microcrack initiation and interaction at the grain boundary but also capture the microcracking behavior inside the grains which is associated with intragranular microcracking. This method has been demonstrated to be capable of simulating the failure behavior and microcracking process of crystalline rocks [*Bahrani and Kaiser*, 2016; *Bahrani et al*., 2014; *Bewick et al*., 2014a, 2014b; *Hofmann et al*., 2015a, 2015b].

2.2. Numerical Model Setup

In this study, the numerical model comprises four minerals (quartz, K-feldspar, plagioclase, and biotite) which is the same as that examined in laboratory tests. Grain sizes of different minerals are generally different. The average grain size R_a of a numerical model is expressed as

$$R_a = \sum_{i=1}^{m} \omega_i r_i, \tag{1}$$

where ω_i and r_i are the volume fraction and mean grain size of different constituent minerals, respectively, and m is the number of associated mineral types.

In order to study the influence of material heterogeneity, which is induced by the variation of grain size distribution, on rock strength and microcracking behavior, a dimensionless heterogeneity index H is defined as

$$H = \sqrt{\sum_{i=1}^{m} \left(\frac{r_i}{R_a} - 1 \right)^2}. \tag{2}$$

By changing the grain size of different minerals that constitute a rock, numerical models with different heterogeneity indices can be generated. According to the definition of the heterogeneity index, a larger heterogeneity index represents a more heterogeneous model. Table 1 shows the mean grain sizes of minerals r_i and the heterogeneity indices H for the six different numerical models investigated in this study. The average grain sizes R_a of the numerical models are basically the same, while the heterogeneity indices range from 0 to 1.12.

In our recent study, the microcracking behavior of Singapore Bukit Timah granite (BTG) was simulated using the PFC2D grain-based model. The studied BTG was composed of approximately 22.3% K-feldspar, 30.4% quartz, 36.3% plagioclase, and 10.7% biotite. It was found from previous laboratory test results that the mineralogical composition had a great influence on the mechanical properties of rocks [*Güneş Yılmaz et al*., 2011; *Přikryl*, 2001; *Sajid et al*., 2016; *Tuğrul and Zarif*, 1999]. To avoid the influence of mineralogical composition on the simulation results in this paper, we assign the content of each mineral with equal value, i.e., 25.0%.

The dimensions of the present generated numerical specimen models are 50 mm in length and 25 mm in width. They are smaller than those experimentally tested (100 mm long and 50 mm wide). According to *Potyondy and Cundall* [2004], if the particle size is relatively small as compared to the size of the model, the scale effect is not significant for modeling rocks in compressive loading conditions. Reducing the size of the numerical model will thus not significantly affect the simulation results but can improve the computing efficiency. The generated numerical specimen models of different heterogeneity indices are presented in Figure 3. Note that when the heterogeneity index is equal to 0, the model is homogeneous, consisting of uniformly packed regular hexagons.

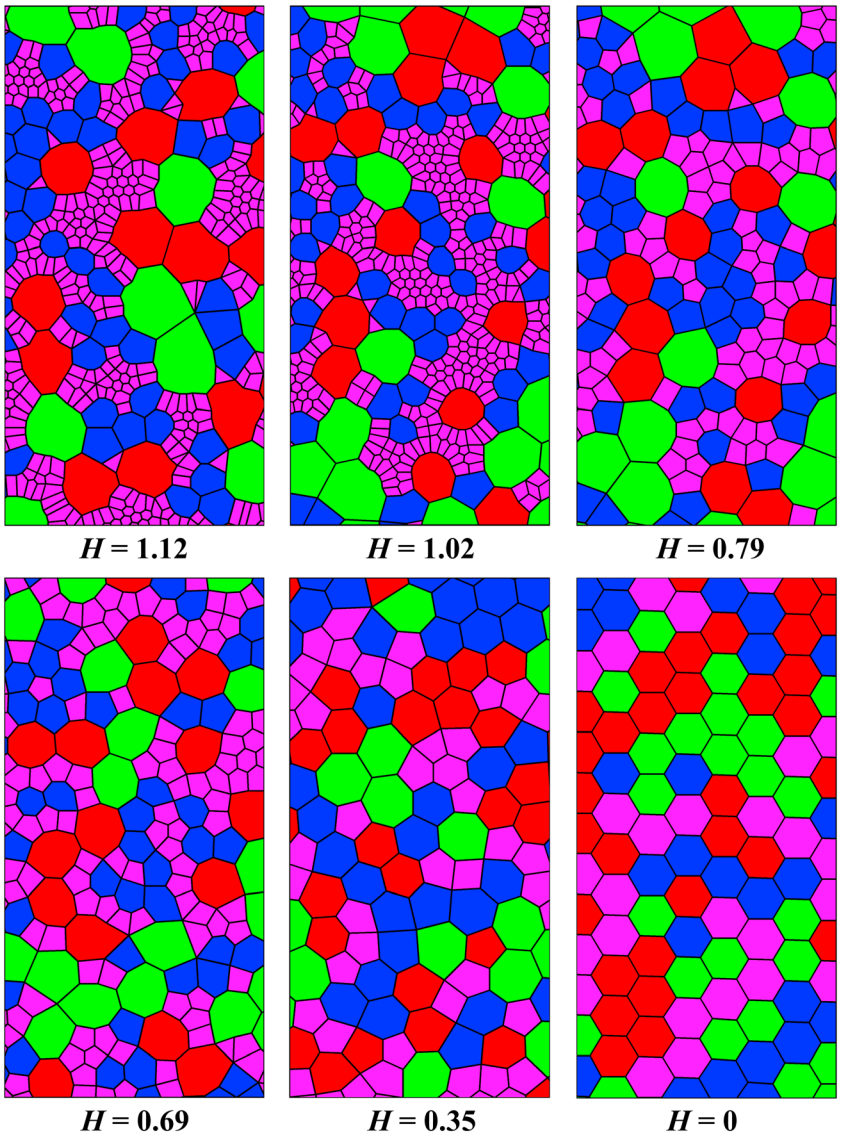

Figure 3. Numerical models with different heterogeneity indices. The colors indicate different mineral types (red = K-feldspar, blue = quartz, green = plagioclase, and magenta = biotite). The specimen dimensions are 50 mm in length and 25 mm in width.

The heterogeneity index reflects the grain size distribution of the numerical model (see Figure 4). The grain size becomes more homogeneous when the heterogeneity index decreases from 1.12 to 0. For comparison, the grain size distribution of the studied BTG (thin solid line) is also shown in Figure 4. The left and right dashed lines represent the minimum and maximum grain size distributions of BTG tested in the laboratory, respectively.

2.3. Calibrated Microparameters

Parameter calibration is a critical step in numerical simulation. However, the general calibration procedure in PFC2D is mainly a trial-and-error process. Many studies have been conducted to examine the relationship between microparameters and macroproperties which can serve as guidance for the selection of parameters for a specific rock type [*Fakhimi and Villegas*, 2007; *Weng and Li*, 2012; *Yoon*, 2007]. To ensure the validation of parameter calibration, a calibration procedure was developed and the microparameters were calibrated to match as many macroproperties of the BTG tested in the laboratory as possible in our recent study. These

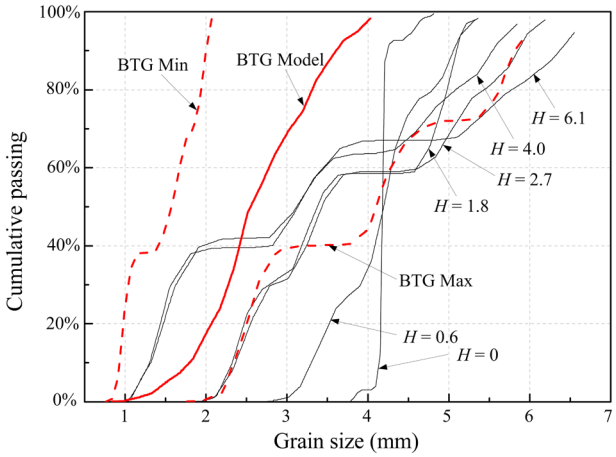

Figure 4. Grain size distributions of numerical models with different heterogeneity indices. The grain size distributions for the Bukit Timah granite (BTG) are shown in red.

macroproperties include direct tensile strength (σ_{dt}), UCS, Young's modulus (E), and compressive strengths under various confining pressures.

The calibration results in our recent study are reproduced in Figure 5. The simulated strength envelope is nonlinear and is comparable with that obtained using Hoek-Brown (H-B) failure criterion. By fitting the test data using H-B failure criterion, the H-B model can well capture the strength behavior of BTG. The fitted UCS (σ_c) and material parameter m_i are 184.7 MPa and 23.2, respectively. The simulated macroproperties are also summarized in Table 2. The results reveal that the errors between the laboratory properties and the simulated values using grain-based model are within ± 6%.

The microparameters for a parallel bond include the size distribution of particles (R_{max}/R_{min} and R_{min}), strength of parallel bond (tensile strength $\bar{\sigma}c$ and cohesion $\bar{C}$), stiffness of particles (k_n and k_s), stiffness of parallel bond ($\bar{k}n$ and $\bar{k}s$), particle contact modulus (E_c), parallel bond modulus ($\bar{E}c$), and friction coefficient between particles (μ). To represent different mechanical properties of the four minerals in this study, the microparameters should be assigned different values for different grains (particles and parallel bonds).

The smooth-joint contact model was first proposed to model the mechanical behavior of joints in fractured rock masses [*Ivars et al.*, 2011]. The smooth-joint contact is assigned to all contacts between particles that lie on opposite side of the joint. After the smooth-joint contacts are assigned, parallel bonds at these contacts are then removed and smooth-joint contacts are imposed in a direction parallel with the joint planes. Once the smooth-joint contact is created, its stiffness properties are assigned as a factor (i.e., stiffness factor) of the stiffness inherited from the contact and the two contacting particles, according to the following equations [*Bahrani et al.*, 2012]:

$$\bar{k}^n = (k_n/A) + \bar{k}_n, \tag{3}$$

$$\bar{k}^s = (k_s/A) + \bar{k}_s, \tag{4}$$

$$A = 2\bar{R}t, \tag{5}$$

$$\bar{R} = \lambda \min\left(R^A, R^B\right), \tag{6}$$

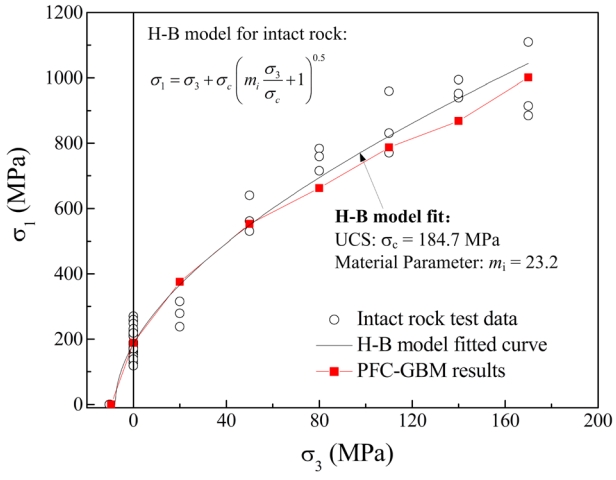

Figure 5. Comparison of the simulated strength envelope with that estimated using Hoek-Brown (H-B) failure criterion.

where $\bar{k}n$ and $\bar{k}s$ are the smooth-joint contact normal stiffness and shear stiffness, respectively, A is the cross sectional area of the smooth-joint contact, t is the disc thickness and equal to 1 for PFC2D problem, $\bar{R}$ is the smooth-joint contact radius (i.e., half length of the smooth-joint contact), which is a multiple, λ, of the two particle radii, R^A and R^B.

Table 3 summarizes the calibrated microparameters for the BTG. The moduli, stiffness ratios, and densities of particles, as well as the moduli, stiffness ratios, tensile strengths, and cohesions of parallel bonds are assigned with different values for the

Table 2. Summary of Results Obtained by Laboratory Tests, H-B Model Fit, and Numerical Simulation[a]

Properties	Laboratory Test Results	H-B Model	Simulation Results	Error (%)
σ_{dt} (MPa)	10.1	/	9.5	−5.94
E (GPa)	35.5	/	35.7	+0.56
UCS (MPa)	186.8	184.7	187.9	+1.73
$\sigma_{1@20MPa}$ (MPa)	315.8	366.4	375.7	+2.54
$\sigma_{1@50MPa}$ (MPa)	576.7	548.8	552.3	+0.64
$\sigma_{1@80MPa}$ (MPa)	752.1	694.5	662.3	−4.64
$\sigma_{1@110MPa}$ (MPa)	837.3	821.6	786.8	−4.24
$\sigma_{1@140MPa}$ (MPa)	995.9	937.0	888.7	−5.51
$\sigma_{1@170MPa}$ (MPa)	1107.5	1044.1	1001.3	−4.10

[a]For direct tensile strength (σ_{dt}) and Young's modulus (E), the error is calculated by ($Value_{simu} - Value_{lab}$)/$Value_{lab}$. For compressive strengths under different confining pressures, the error is calculated by ($Value_{simu} - Value_{HB}$)/$Value_{HB}$.

four different minerals. The calibrated microparameters for different minerals are comparable with the mineral properties suggested by *Bass* [1995]. For example, the quartz has the highest strength, modulus, and cohesion, and the biotite has the highest density. All smooth-joint contacts of different mineral contacts are assigned with the same set of parameters to reduce the number of calibrated microparameters and computational iterations. The microparameters listed in Table 3 were proven capable of modeling strength and deformation behavior and the associated microcracking process of BTG under different loading conditions in our recent study.

Results obtained from previous three-dimensional compressive laboratory tests were used to calibrate the microparameters of the two-dimensional PFC grain-based model in this study. This approach is also used in several other studies [*Bahrani et al*., 2014; *Hofmann et al*., 2015a; *Yang et al*., 2014]. Though the loading condition in conventional triaxial compression tests is different from that of two-dimensional biaxial tests using PFC2D, the approach is proven capable to simulate the microcracking behavior of BTG. It should be noted that there are limitations of using PFC2D to account for three-dimensional phenomena observed in laboratory tests. However, the grain-based model is easily incorporated in PFC2D, and insights can be obtained from numerical simulations in PFC2D.

In the following section, numerical simulations of the models under uniaxial compression, confining pressures of 10 MPa and 20 MPa, and direct tension are conducted based on the microparameters shown in

Table 3. Summary of Calibrated Microparameters for BTG

Microparameters	Values			
	K-Feldspar	Quartz	Plagioclase	Biotite
Microproperties of the Minerals				
Minimum particle radius, R_{min} (mm)	0.15	0.15	0.15	0.15
Particle-size ratio, R_{max}/R_{min}	1.66	1.66	1.66	1.66
Particle-particle contact modulus, E_c (GPa)	20	32	26	12
Contact normal to shear stiffness ratio, k_n/k_s	1.6	1.0	1.7	1.1
Particle friction coefficient, μ	1.2	1.2	1.2	1.2
Particle density, ρ (kg/m^3)	2600	2650	2600	2850
Parallel bond radius multiplier, λ	1	1	1	1
Parallel bond modulus, $\bar{E}c$ (GPa)	20	32	26	12
Parallel bond normal to shear stiffness ratio, $\bar{k}n/\bar{k}s$	1.6	1.0	1.7	1.1
Parallel bond tensile strength, $\bar{\sigma}c$ (MPa)	376	391	376	360
Parallel bond cohesion, $\bar{C}$ (MPa)	376	391	376	360
Parallel bond friction angle, ϕ (deg)	30	30	30	30
Microproperties of the Mineral Boundaries (Smooth-Joint Contacts)				
Smooth-joint contact normal stiffness factor, α ($\bar{k}n$)	0.6			
Smooth-joint shear normal stiffness factor, α ($\bar{k}n/\bar{k}s$)	0.8			
Smooth-joint bond tensile strength, σ_b (MPa)	14			
Smooth-joint bond cohesion, C_b (MPa)	130			
Smooth-joint bond friction angle, ϕ_b (deg)	30			
Smooth-joint bond friction coefficient, μ_b	1.2			

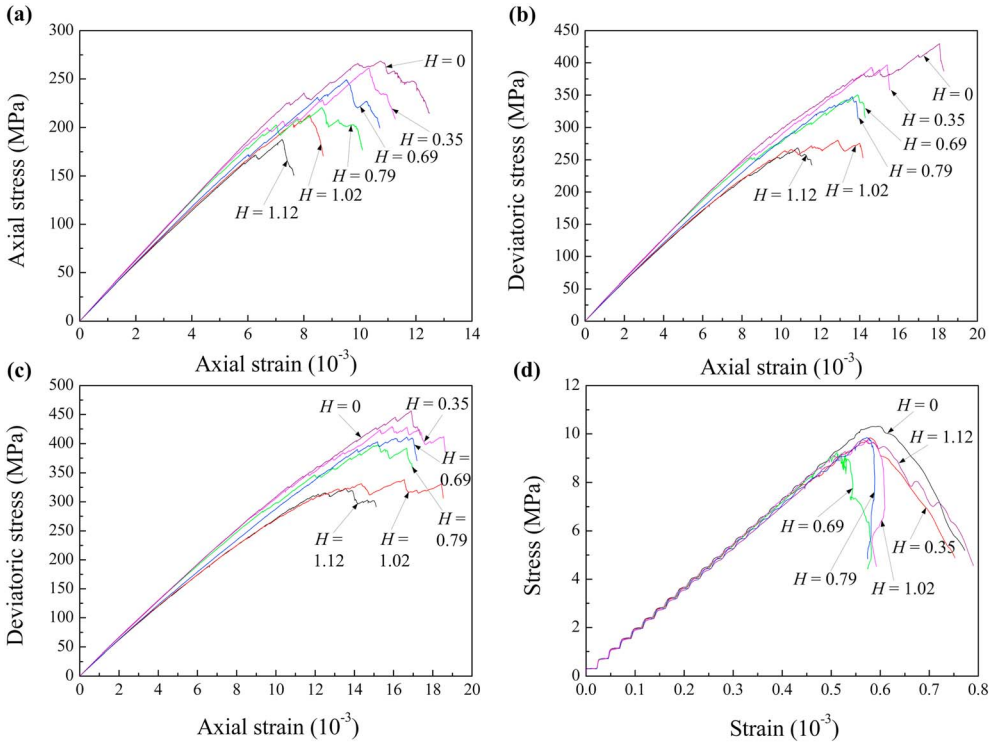

Figure 6. Simulated stress-strain curves of numerical models under different loading conditions. (a) Uniaxial compression. (b) Compression under confining pressure of 10 MPa. (c) Compression under confining pressure of 20 MPa. (d) Direct tension.

Table 3. Afterward, influence of material heterogeneity on the strength evolution and microcracking behavior of BTG will be analyzed and discussed.

Due to the fact that the particles are arbitrarily assembled in the initial disc packing stage and also in the base material generation stage (see Figure 1), the heterogeneity induced from the difference in assembled particles of the numerical model is suspected to have an influence on the simulation results. As such, before the numerical simulations are conducted, the effect of this particle assembly-induced heterogeneity is examined. The numerical model with heterogeneity index equal to 1.12 is generated 10 times. When the mean grain sizes of minerals and mineralogical compositions are fixed, the generated numerical models are found to be identical. After running the generated models with the same parameters listed in Table 3, the simulated stress-strain behaviors and microcracking evolutions are found to be identical for the 10 models. Therefore, the particle assembly-induced heterogeneity has no significant influence on the simulation results in this study.

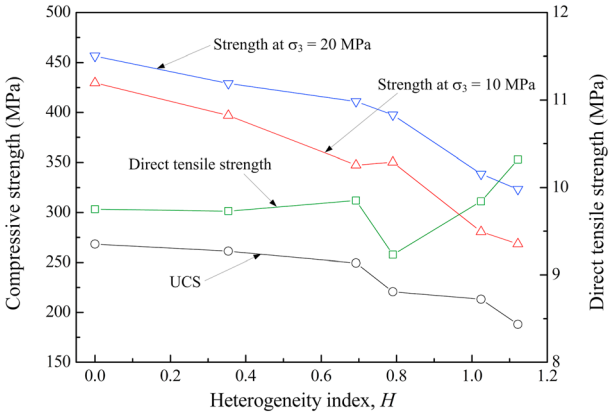

Figure 7. Strength evolutions of numerical models with the heterogeneity index.

3. Results and Discussion

3.1. Deformation Behavior and Rock Strength

The influence of grain size heterogeneity on the simulated stress-strain responses and rock strength evolutions of the numerical models will be examined and discussed in this section.

3.1.1. Stress-Strain Response

The simulated stress-strain responses of the numerical models under different

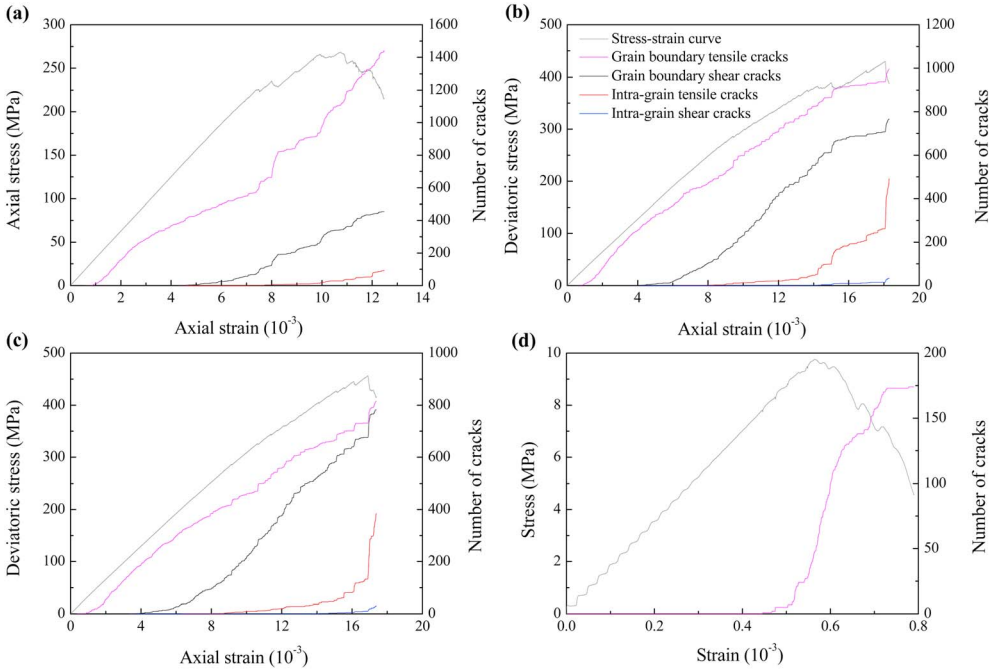

Figure 8. Evolution of microcracks during loading of specimen HE6 ($H = 0$) under different conditions. (a) Uniaxial compression. (b) Compression under confining pressure of 10 MPa. (c) Compression under confining pressure of 20 MPa. (d) Direct tension.

loading conditions are shown in Figure 6. The results reveal that the heterogeneity has a significant effect on the simulated stress-strain curves under compressive conditions. Under uniaxial compression, the stress-strain curves generally show a brittle manner (see Figure 6a). When the models are loaded under the confining pressures of 10 MPa and 20 MPa (see Figures 6b and 6c), the stress-strain curves become more ductile than those under uniaxial compression. In general, the elastic moduli of the numerical models under compressive loading increases as the model progresses from heterogeneous to homogeneous. However, under direct tension condition (see Figure 6d), the heterogeneity does not have an obvious influence on the simulated stress-strain curves, especially in the prepeak deformation stage.

3.1.2. Rock Strength Evolution

The strength variations of the numerical models with the heterogeneity indices are illustrated in Figure 7. The material heterogeneity also has a great effect on the rock strength under compressive loadings. The compressive strength gradually decreases as the heterogeneity index increases from 0 to 1.12; i.e., the more heterogeneous the numerical model is, the lower the compressive strengths will be. On the other hand, the simulated direct tensile strength slightly increases with the increase of heterogeneity index from 0 to 1.12. However, there is a drop of the strength when the heterogeneity index is equal to 0.79. *Mohsen and Martin* [2014] studied the heterogeneity effect on the crack initiation stress and the uniaxial compressive strength (UCS) of low-porosity crystalline rock using grain-based model in UDEC. They also found that the more homogeneous the numerical model was, the higher the crack initiation stress and UCS would be.

3.2. Microcracking Behavior

In the following discussion, the influence of material heterogeneity, which is induced by the variation of grain size distribution, on the microcracking behavior (i.e., number, orientation, and position of the induced microcracks) will be analyzed.

3.2.1. Number of Microcracks

Numerous previous studies have revealed that the number of induced microcracks will gradually increase with the increase of the applied stress [*Blake and Faulkner*, 2016; *Brace et al*., 1966; *Hadley*, 1976; *Tapponnier and Brace*, 1976; *Wong*, 1982b]. In the present study, as an example, the evolutions of crack count of different types of microcracks, namely, grain boundary microcracks and intragrain microcracks, during loading of the numerical model HE6 ($H = 0$) are shown in Figure 8. Both types of microcracks

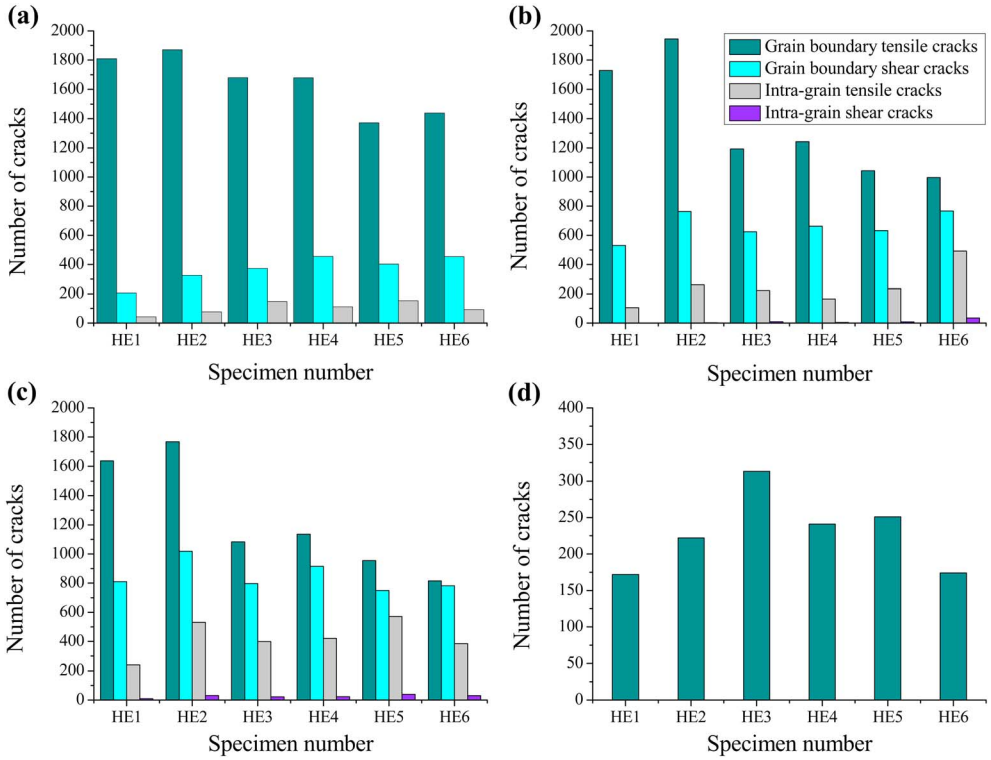

Figure 9. Number of different types of generated microcracks for different numerical models. (a) Uniaxial compression. (b) Compression under confining pressure of 10 MPa. (c) Compression under confining pressure of 20 MPa. (d) Direct tension.

gradually increase in number in response to loading. Under uniaxial compression (Figure 8a), most of the generated microcracks are grain boundary tensile cracks, while no intragrain shear cracks develop during compression. Some intragrain shear cracks develop during loading when the numerical model is loaded under confined compression (Figures 8b and 8c). In addition, the development of grain boundary shear cracks under confined compression is much more favored as compared to that under unconfined compression. In all compressive loading conditions, the grain boundary tensile cracks dominate among the generated microcrack types, indicating that the failure mechanism is attributed mainly to tensile cracking under low confining pressures.

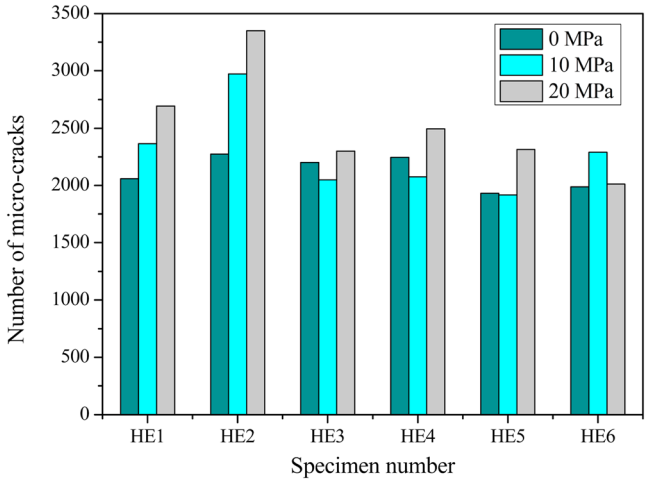

Figure 10. Summary of total number of microcracks generated in different numerical models under different confining pressures.

As shown in Figure 8d, only grain boundary tensile cracks are detected during the entire loading stage of the model under direct tension condition. These cracks initiate at a stress level approximately 80% of the peak strength, which then multiply rapidly upon approaching the peak strength.

Figure 9 presents the number of four different types of microcracks at the end of the loading process of the numerical models under different loading conditions. It is found that the number of grain boundary tensile cracks generally decreases with the decrease of heterogeneity index from 1.12 to 0 under compressive compression. However, there is no obvious

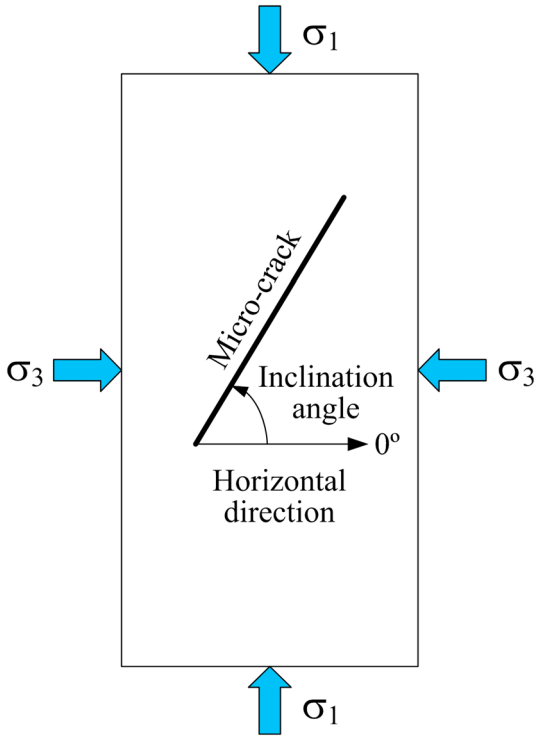

Figure 11. Definition of inclination angle of the generated microcracks in the numerical model.

trend for the development of other types of microcracks. Similarly, under the direct tension condition, no obvious relation is found between the number of grain boundary tensile cracks and the heterogeneity index. For the numerical model with the same heterogeneity index, fewer grain boundary tensile cracks are produced with the increase of confining pressure, while the generation of the other three types of microcracks is more favored as the confining pressure increases.

The total number of generated microcracks for different numerical models is also computed and summarized in Figure 10. The results reveal that when the heterogeneity index is large (i.e., HE1 and HE2), the total number of microcracks increases with the increase of confining pressure. However, as the heterogeneity index becomes lower, the total numbers of generated microcracks are very similar for different confining pressures. Under the same confining pressure, the heterogeneity has no significant effect on the total number of generated microcracks.

3.2.2. Orientation of Microcracks

The heterogeneity induced by variation of grain size distribution has a great influence on the orientation of generated microcracks. The influence of heterogeneity on the inclination angle of microcracks is discussed in this subsection. As shown in Figure 11, the inclination angle (0 to 180°) is defined as the angle between the horizontal direction and the microcracking direction in an anticlockwise direction. For example, if a microcrack orients in the vertical loading direction, the inclination angle is equal to 90°.

Figure 12 illustrates the orientation distribution of generated grain boundary microcracks for numerical models with different heterogeneity indices under uniaxial compression. The results reveal that the orientation of grain boundary microcracks is significantly affected by the grain size distribution induced heterogeneity, which is associated with the geometry of assembled grain structure of the numerical model. When the heterogeneity index is large, the grain boundary microcracks are generated approximately parallel to the vertical direction. As the heterogeneity index decreases, although most of the generated grain boundary microcracks

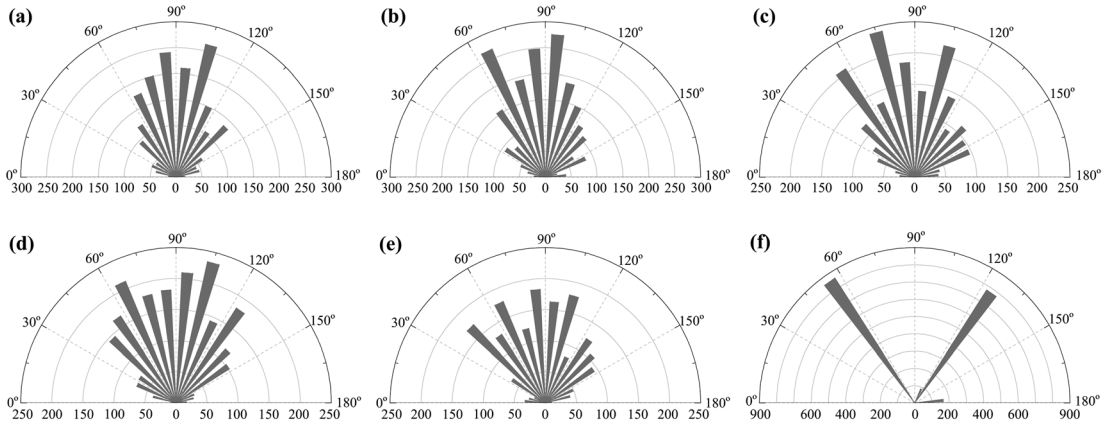

Figure 12. Orientation distribution of the generated grain boundary microcracks in the numerical models with different heterogeneity indices under uniaxial compression. (a) HE1: $H = 1.12$. (b) HE2: $H = 1.02$. (c) HE3: $H = 0.79$. (d) HE4: $H = 0.69$. (e) HE5: $H = 0.35$. (f) HE6: $H = 0$.

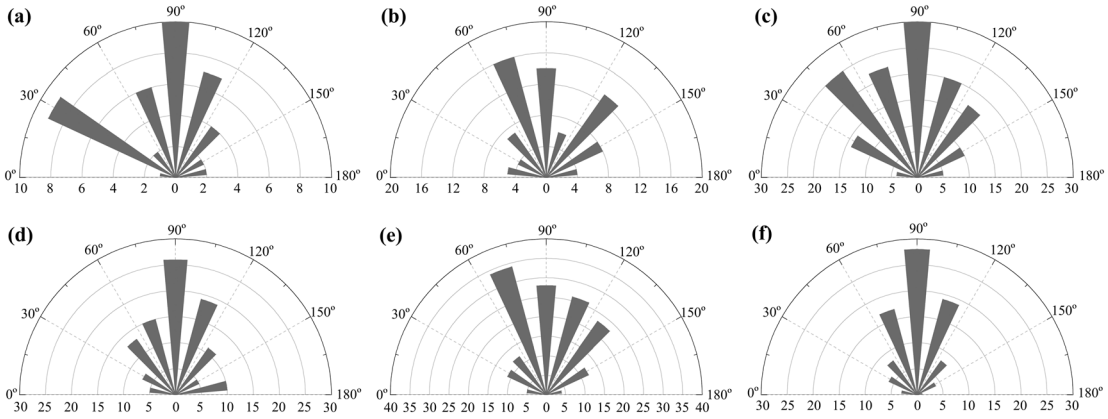

Figure 13. Orientation distribution of the generated intragrain microcracks in the numerical models with different heterogeneity indices under uniaxial compression. (a) HE1: $H = 1.12$. (b) HE2: $H = 1.02$. (c) HE3: $H = 0.79$. (d) HE4: $H = 0.69$. (e) HE5: $H = 0.35$. (f) HE6: $H = 0$.

are oriented in the vertical direction, more and more microcracks are found to be inclined at about 60 to 75° and 105 to 120°. When the numerical model is homogeneous ($H = 0$), most of the grain boundary microcracks are generated at about 60° and 120°. The phenomenon is mainly due to the general association of the grain boundary microcracks and the grain interfaces in the generated numerical models. As shown in Figure 3, as the numerical model becomes more homogeneous, more grain interfaces tend to be inclined at about 60 to 75° and 105 to 120°.

The orientation distribution of generated intragrain microcracks of different numerical models under uniaxial compression are presented in Figure 13. The heterogeneity induced by variation of grain size distribution does not have a pronounced influence on the orientation of intragrain microcracks, as compared with the results of grain boundary microcracks. Most of the generated intragrain microcracks incline approximately parallel or slightly inclined to the vertical loading direction.

Figure 14 presents the variations of orientation of grain boundary microcracks and intragrain microcracks with the confining pressure for the numerical model with the heterogeneity index equal to 0.69. The rose diagrams reveal that the orientation of grain boundary microcracks are generally the same under different confining pressures, indicating that the confinement does not have a significant influence. On the other hand, the orientation of intragrain microcracks seems to be greatly affected by the confinement. When the numerical model is loaded under uniaxial compression, most of the intragrain microcracks are generated along the vertical direction. With increase of the confining pressure, more intragrain microcracks are found to incline at about 30° along the loading direction.

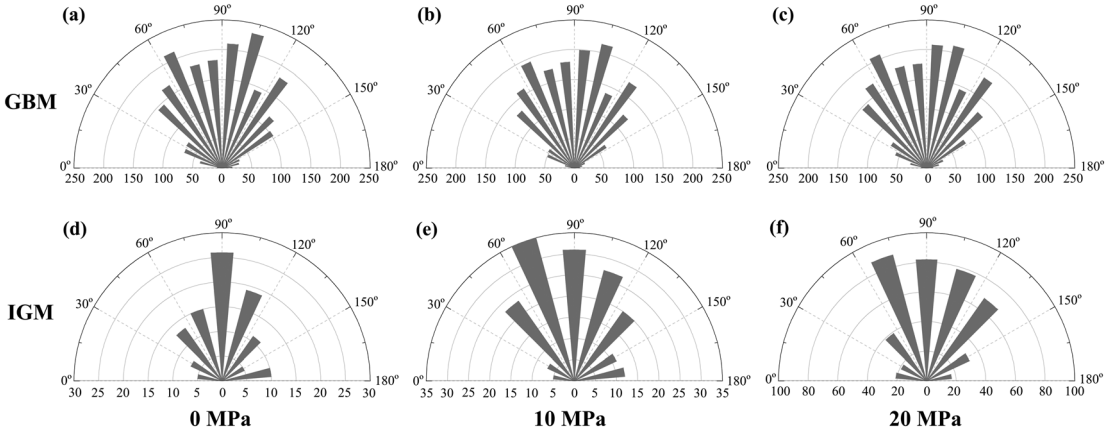

Figure 14. Orientation distribution of two types of microcracks in the numerical model HE4 ($H = 0.69$) under various confining pressures. Grain boundary microcracks under (a) uniaxial compression, (b) confining pressure of 10 MPa, and (c) confining pressure of 20 MPa. Intragrain microcracks under (d) uniaxial compression, (e) confining pressure of 10 MPa, and (f) confining pressure of 20 MPa. (GBM: grain boundary microcrack; IGM: intragrain microcrack).

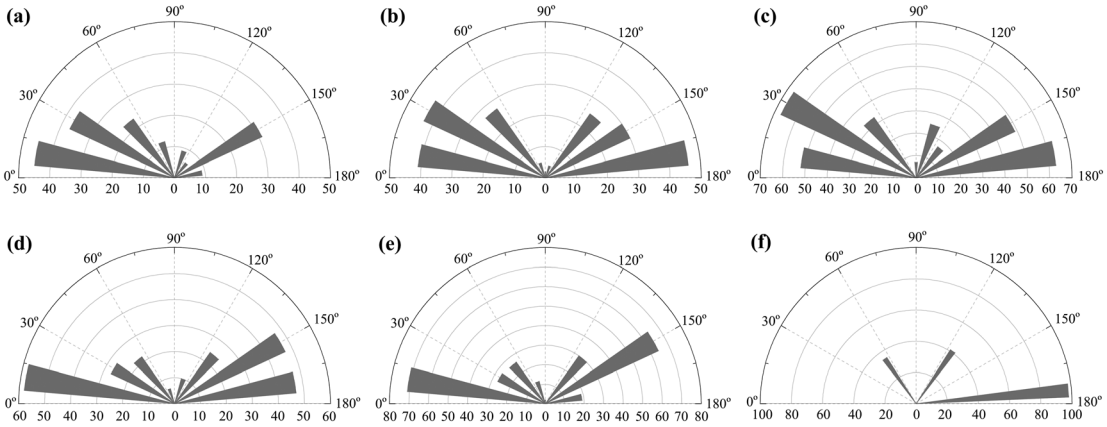

Figure 15. Orientation distribution of the generated microcracks in the numerical models with different heterogeneity indices under direct tension. (a) HE1: $H = 1.12$. (b) HE2: $H = 1.02$. (c) HE3: $H = 0.79$. (d) HE4: $H = 0.69$. (e) HE5: $H = 0.35$. (f) HE6: $H = 0$.

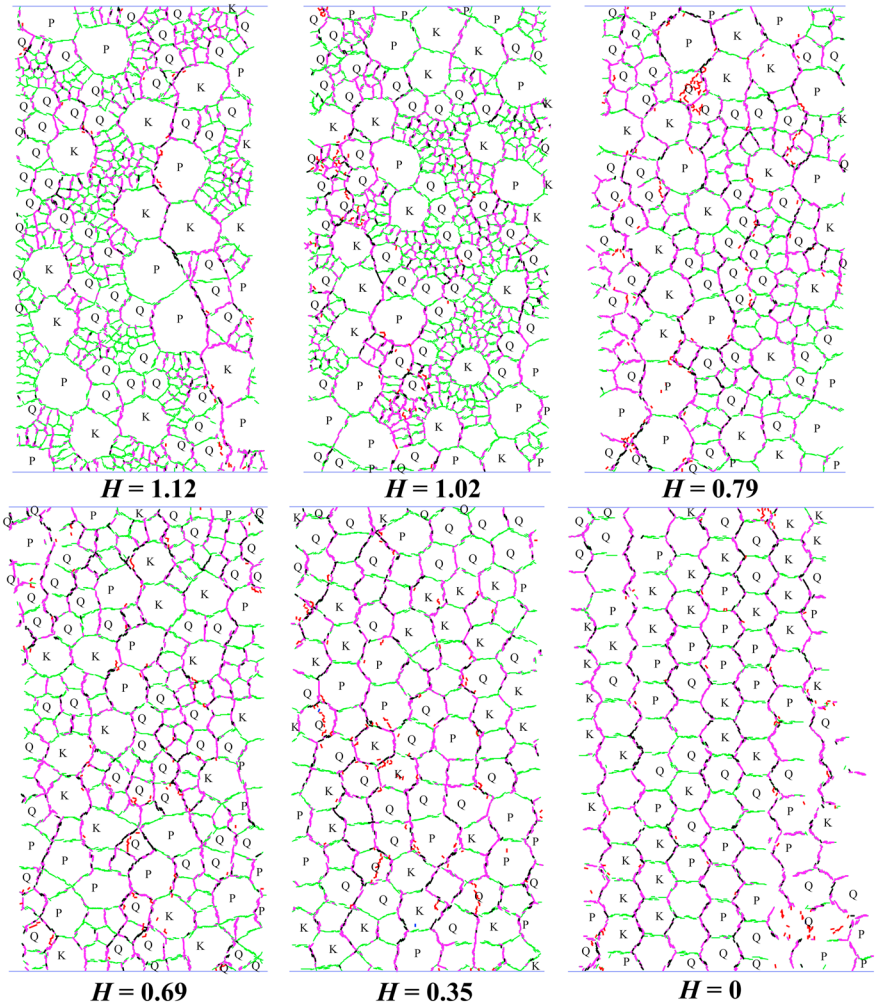

Figure 16. Microcracking behavior of the numerical models with different heterogeneity indices under uniaxial compression. The different minerals are identified (Q: quartz, K: K-feldspar, P: plagioclase, and biotite is not labeled). Green segments represent grain boundaries, magenta and black segments represent grain boundary tensile and shear cracks, respectively, and red segments represent intragrain tensile cracks.

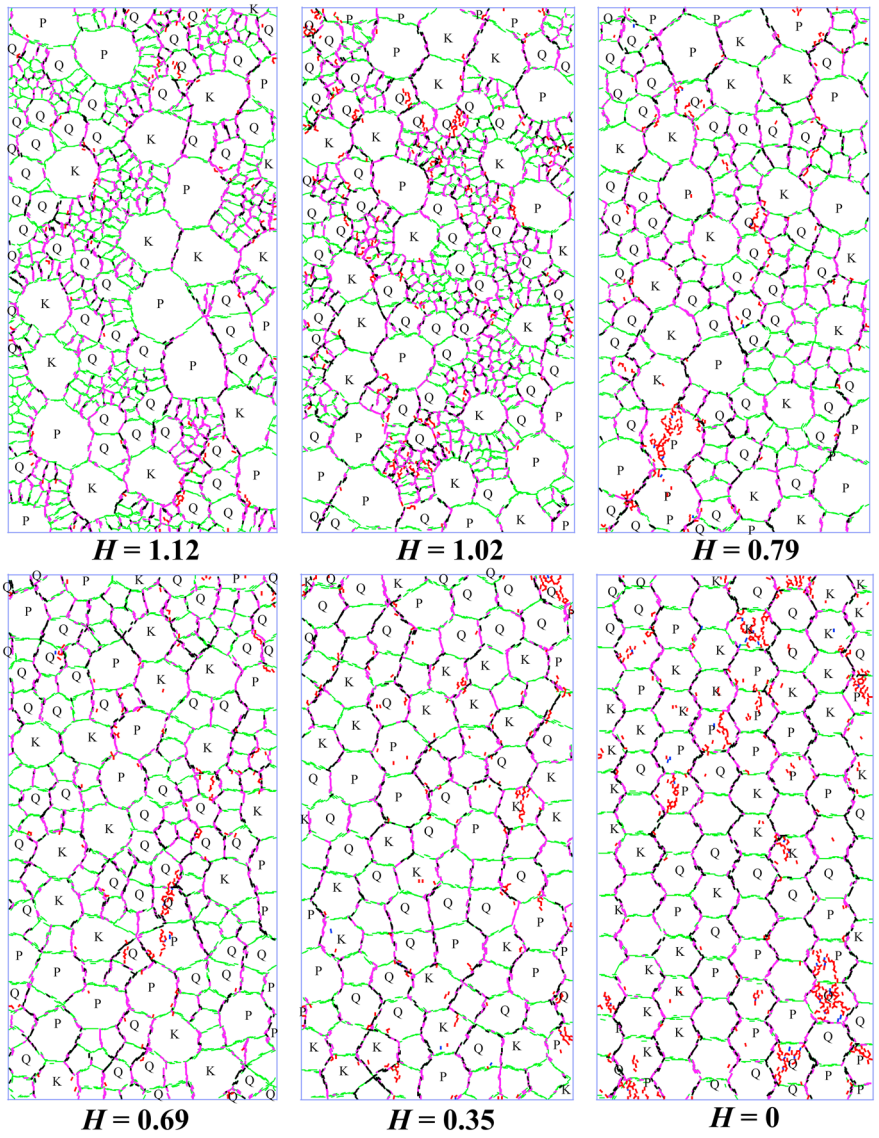

Figure 17. Microcracking behavior of the numerical models with different heterogeneity indices under the confining pressure of 10 MPa. The different minerals are identified (Q: quartz, K: K-feldspar, P: plagioclase, and biotite is not labeled). Green segments represent grain boundaries, magenta and black segments represent grain boundary tensile and shear cracks, respectively, and red and blue segments represent intragrain tensile and shear cracks, respectively.

Figure 15 illustrates the orientations of the generated microcracks for different numerical models under direct tension. The results reveal that the material heterogeneity has a great influence on the orientations of the generated microcracks in direct tensile loading condition. When the heterogeneity index is high, most of the generated microcracks are approximately perpendicular or inclined at about 60° to the vertical loading direction. As the heterogeneity index gradually decreases, most of the generated microcracks are inclined at about 60 or 80° to the vertical direction. Most of the generated microcracks are approximately perpendicular to the vertical loading direction when the numerical model becomes highly homogeneous.

3.2.3. Pattern of Microcracks

The spatial distributions of different types of microcracks for numerical models with different heterogeneity indices under uniaxial compression are presented in Figure 16. The results reveal that the pattern of generated microcracks varies with the heterogeneity index. When the heterogeneity index is relatively high, the generated microcracks are generally uniformly distributed in the model, with the orientation of microcracks varying in a relatively large range. As the numerical model becomes more homogeneous, the interaction of

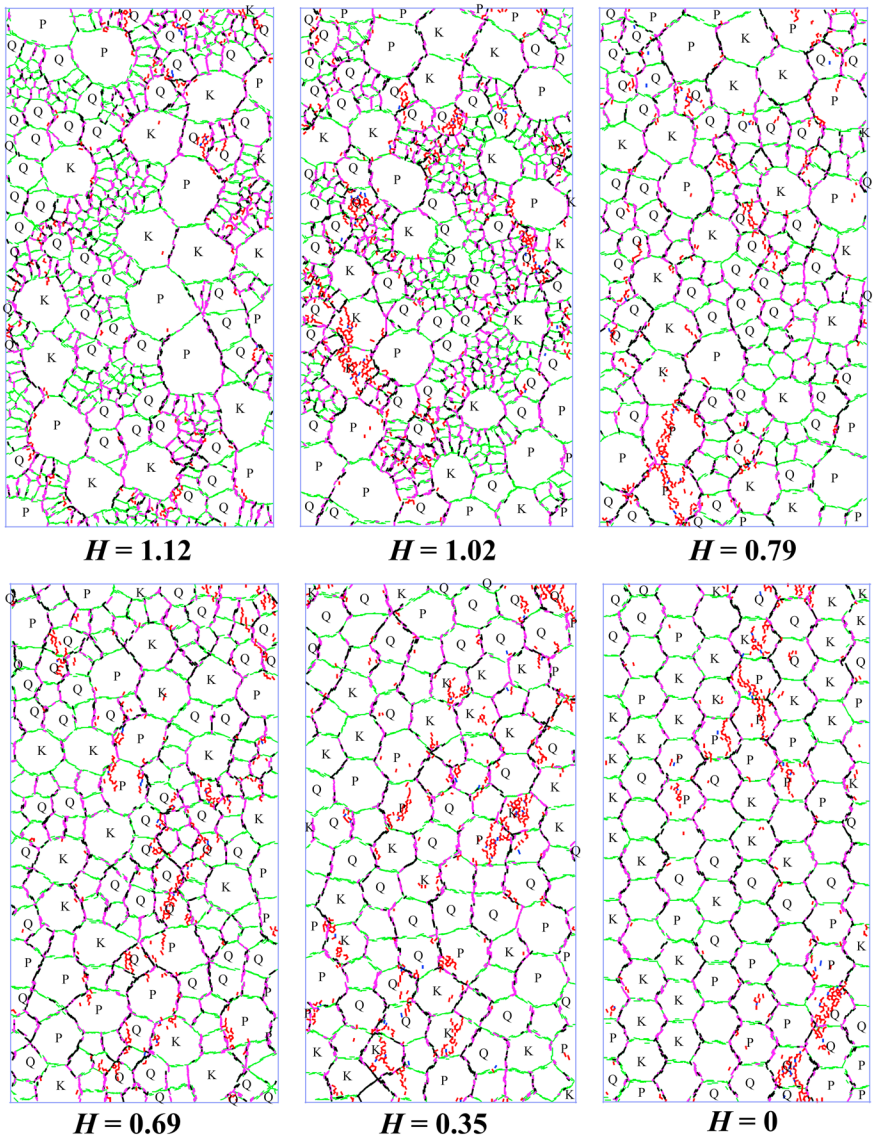

Figure 18. Microcracking behavior of the numerical models with different heterogeneity indices under the confining pressure of 20 MPa. The different minerals are identified (Q: quartz, K: K-feldspar, P: plagioclase, and biotite is not labeled). Green segments represent grain boundaries, magenta and black segments represent grain boundary tensile and shear cracks, respectively, and red and blue segments represent intragrain tensile and shear cracks, respectively.

generated microcracks tends to form more macroscopic fractures which are oriented approximately in the vertical direction. Because the homogeneous numerical model ($H = 0$) is uniformly assembled with regular hexagons, when the numerical model is loaded, the microcracks are generally generated along the subvertical grain interfaces, which will eventually form vertical macroscopic fractures. The lateral dilation in this condition is much larger than those with large heterogeneity indices.

Figure 17 illustrates the distributions of different types of microcracks for numerical models with different heterogeneity indices under the confining pressure of 10 MPa. Similarly, the heterogeneity of the numerical model has a significant effect on the pattern of the generated microcracks. When the heterogeneity index is large, more grain boundary tensile cracks develop in the model. The generated microcracks are distributed more uniformly than in the models with much lower heterogeneity indices. As the numerical model becomes more homogeneous, more intragrain cracks develop in the model. In addition, the development of intragrain cracks is more favored under the confining pressure of 10 MPa as compared to the results under uniaxial compression.

Table 4. Number of Intragrain Tensile and Shear Microcracks Generated in Different Minerals Under Compressive Loading Condition[a]

σ_3 (MPa)	Heterogeneity Index, H	Number of Grains				Number of Intragrain Tensile Cracks					Number of Intragrain Shear Cracks				
		Q	K	P	B	Q	K	P	B	Total	Q	K	P	B	Total
0	1.12	14	48	10	336	15	7	7	12	41	0	0	0	0	0
	1.02	17	46	18	348	23	3	8	39	73	0	0	0	0	0
	0.79	17	48	17	94	74	13	31	25	143	0	0	0	0	0
	0.69	16	48	18	119	55	20	14	20	109	0	0	0	0	0
	0.35	27	34	16	48	68	29	25	26	148	1	1	0	0	2
	0	32	25	25	27	38	16	16	15	85	1	0	0	0	1
10	1.12	14	48	10	336	43	6	14	39	102	0	0	0	0	0
	1.02	17	46	18	348	89	19	26	117	251	2	0	0	0	2
	0.79	17	48	17	94	74	19	97	31	221	4	0	5	0	9
	0.69	16	48	18	119	75	13	40	36	164	3	0	2	0	5
	0.35	27	34	16	48	83	64	40	45	232	3	3	2	0	8
	0	32	25	25	27	128	119	172	65	484	12	7	9	5	33
20	1.12	14	48	10	336	92	23	28	87	230	9	0	0	0	9
	1.02	17	46	18	348	154	119	39	202	514	19	8	4	0	31
	0.79	17	48	17	94	116	33	164	75	388	11	1	8	2	22
	0.69	16	48	18	119	170	29	92	114	405	10	2	5	6	23
	0.35	27	34	16	48	146	200	123	88	557	12	13	8	6	39
	0	32	25	25	27	148	59	139	37	383	14	4	10	2	30

[a]Q: quartz, K: K-feldspar, P: plagioclase, and B: biotite.

Due to the applied confining pressure, the lateral dilation of the numerical model during loading is constrained. The high stress concentration in the homogeneous model ($H = 0$) will induce intensive microcracking inside the grains. Under the confining pressure of 10 MPa, the grain boundary cracks still dominate among the generated microcracks. Because the grain boundary cracks are associated with grain interfaces, with fewer intragrain cracks developed, the macroscopic fractures of numerical models with higher heterogeneity indices are still basically in the vertical direction. However, as the heterogeneity index becomes smaller, the interaction of grain boundary cracks and more developed intragrain cracks will result in more prominent macroscopic shear bands.

The distributions of different types of microcracks for numerical models with different heterogeneity indices under the confining pressure of 20 MPa are shown in Figure 18. As compared with the results under uniaxial compression and the confining pressure of 10 MPa, more intragrain cracks develop in the model due to the higher applied confining pressure. When the crack density is sufficiently high, the interaction and coalescence of grain boundary microcracks and intragrain microcracks lead to the formation of macroscopic shear bands. The results are in good agreement with microscopic observation of the Westerly granite by *Moore and Lockner* [1995]. When the heterogeneity index is large, the generated microcracks are found to be relatively uniform. As the numerical model becomes more homogeneous, more intragrain cracks develop in the model and the induced macroscopic shear band is more prominent than the results of numerical models with much higher heterogeneity indices.

Because all of the smooth-joint contacts which are associated with the grain boundaries (grain interfaces) are assigned with the same set of microparameters (see Table 3), the generated grain boundary cracks are basically uniformly distributed in different mineral-mineral contacts under compressive loading. However, the parallel bonds for different minerals which are associated with intragrain cracking are assigned with different sets of microparameters. The properties of intragrain cracks under compressive loading are retrieved from the numerical results and discussed as follows.

Table 4 summarizes the identified intragrain cracks in different minerals under compressive loading condition. The results reveal that with the increase of the confining pressure, the number of generated intragrain cracks for different numerical models gradually increase. For numerical models under the same confining pressure, as the model becomes more homogeneous, more intragrain cracks are formed, even though fewer grains are generated. The high capacity of sustaining microcracking contributes to high rock strength of the

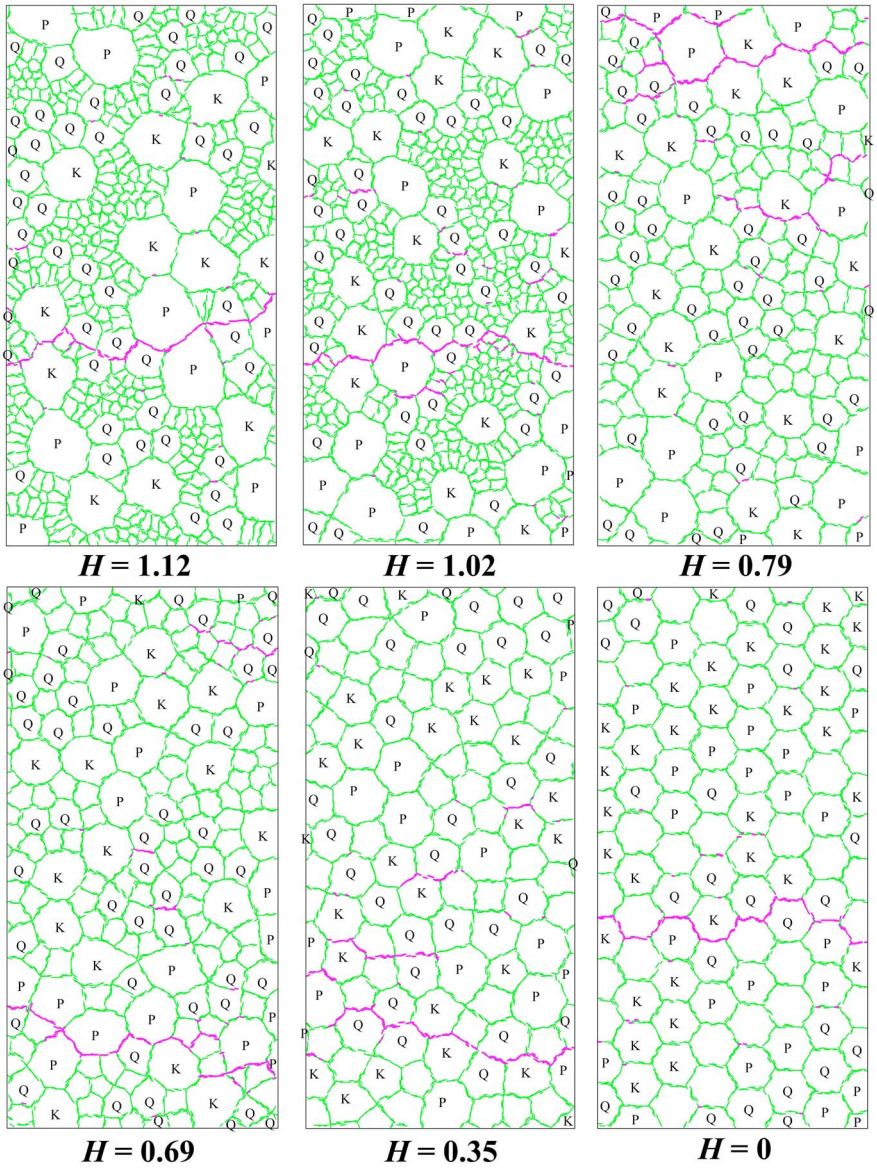

Figure 19. Microcracking behavior of the numerical models with different heterogeneity indices under direct tension. The different minerals are identified (Q: quartz, K: K-feldspar, P: plagioclase, and biotite is not labeled). Green segments represent grain boundaries and magenta segments represent grain boundary tensile cracks.

numerical model. That is why the rock strength of homogeneous model is higher than that of heterogeneous model (section 3.1.2).

It is also seen from Table 4 that most of the intragrain cracks (both tensile and shear) generally develop in quartz (except the numerical models with heterogeneity indices equal to 0.35 and 0.79 under the confining pressure of 20 MPa). This is mainly due to the fact that the particle-particle contact modulus, and parallel bond modulus and strength in the quartz mineral are assigned with the highest value as compared with the values of other minerals (see Table 3). Many researchers investigated the microcracking behavior of crystalline rocks and found that the intragrain cracks occurred mostly in quartz grains [*Akesson et al.*, 2004; *Moore and Lockner*, 1995; *Peng and Johnson*, 1972; *Sprunt and Brace*, 1974; *Tapponnier and Brace*, 1976; *Tullis and Yund*, 1977]. These observations are in good agreement with the simulation results in this study.

Figure 19 presents the distributions of generated microcracks for numerical models with different heterogeneity indices under direct tension. For all numerical models, the coalescence of grain boundary tensile cracks

will eventually form a macroscopic fracture which is approximately perpendicular to the vertical direction. However, the position of the generated macroscopic fracture varies with the heterogeneity indices. When the heterogeneity index is large or equal to 0, the macroscopic fracture develops in the middle portion of the model. On the other hand, when the heterogeneity index is at a moderate value, the macroscopic fracture appears close to the top/bottom end of the numerical model. Meanwhile, when the heterogeneity index is not equal to 0, the generated macroscopic fractures tend to be along the minerals with large grain size. In other words, the section of macroscopic fracture is generally associated with the smallest number of adjacent mineral grains/boundaries.

4. Conclusions

This paper numerically investigates the influence of one aspect of material heterogeneity with respect to grain size variation on the strength and deformation behavior and the associated microcracking process of a crystalline rock containing quartz, K-feldspar, plagioclase, and biotite. A heterogeneity index is defined to quantity the grain size distribution induced material heterogeneity. By using the defined heterogeneity index, the material heterogeneity is explicitly incorporated into the PFC2D numerical models adopting a grain-based modeling approach. The numerical models under different loading conditions, namely, uniaxial compression, compressions under confining pressures of 10 MPa and 20 MPa, and direct tension are then investigated.

The simulation results reveal that the material heterogeneity has a significant influence on the simulated stress-strain responses and rock strength. Under compressive loading, the peak strength and the elastic modulus in general increase as the numerical model gradually progresses from heterogeneous to homogeneous. A brittle to ductile transition behavior is observed in the simulated stress-strain curves as the applied confining pressure increases. However, under direct tension condition, the material heterogeneity seems to have no significant influence on the mechanical behavior.

The microcracking behavior is also found to be greatly affected by material heterogeneity. Under compressive loading, as the numerical model becomes more homogeneous, the number of generated grain boundary tensile cracks gradually decreases and the number of intragrain cracks (both tensile and shear) increases. However, the total number of generated microcracks seems not to be influenced by heterogeneity. The orientation of grain boundary microcracks is mainly controlled by the geometry of assembled grain structure of the numerical specimen model, while the orientation of intragrain microcracks is to a large degree influenced by the confinement. The results also reveal that the development of intragrain cracks (both tensile and shear) is much more favored in quartz than in the other minerals, which is in good agreement with the previous observations in laboratory tests. Only grain boundary tensile cracks are produced when the numerical models are loaded in direct tension. Material heterogeneity has a more significant influence on the position of eventual macroscopic fracture rather than the total number of generated microcracks.

To conclude, this study focuses on the issues of material heterogeneity at mineral scale. This study reveals that the material heterogeneity has a significant influence on the strength and deformation behavior and the associated microcracking process of crystalline rocks. As such, heterogeneity should be carefully taken into consideration in numerical study of the mechanical behavior of crystalline rocks under different loading conditions.

Acknowledgments

The support from the Singapore Academic Research Fund Tier 1 grant (RG112/14) is gratefully acknowledged. The first author acknowledges the support from the National Natural Science Foundation of China (grant 51609178). The second author also acknowledges the support from the Start-up fund, and the Seed Funding Program for Basic Research for New Staff at the University of Hong Kong. The authors would like to thank the Associate Editor and the two anonymous reviewers for their constructive comments and suggestions which greatly improved the quality of the manuscript. The data for this paper are available by contacting the corresponding author at lnywong@hku.hk or the first author at jun.peng@whu.edu.cn.

References

Akesson, U., J. Hansson, and J. Stigh (2004), Characterisation of microcracks in the Bohus granite, western Sweden, caused by uniaxial cyclic loading, *Eng. Geol.*, *72*(1–2), 131–142, doi:10.1016/j.enggeo.2003.07.001.

Bahrani, N., and P. K. Kaiser (2016), Numerical investigation of the influence of specimen size on the unconfined strength of defected rocks, *Comput. Geotech.*, *77*, 56–67, doi:10.1016/j.compgeo.2016.04.004.

Bahrani, N., D. Potyondy, and M. Pierce (2012), Simulation of Brazilian test using PFC2D grain-based model, in *Proceedings of 21st Canadian Rock Mechanics Symposium*, pp. 485–493, Edmonton, Canada.

Bahrani, N., P. K. Kaiser, and B. Valley (2014), Distinct element method simulation of an analogue for a highly interlocked, non-persistently jointed rockmass, *Int. J. Rock Mech. Min.*, *71*, 117–130, doi:10.1016/j.ijrmms.2014.07.005.

Bass, J. D. (1995), Elasticity of minerals, glasses, and melts, in *Mineral Physics & Crystallography: A Handbook of Physical Constants*, edited by T. J. Ahrens, pp. 45–63, AGU, Washington, D. C., doi:10.1029/RF002p0045.

Bewick, R. P., P. K. Kaiser, W. F. Bawden, and N. Bahrani (2014a), DEM simulation of direct shear: 1. Rupture under constant normal stress boundary conditions, *Rock Mech. Rock Eng.*, *47*(5), 1647–1671, doi:10.1007/s00603-013-0490-8.

Bewick, R. P., P. K. Kaiser, and W. F. Bawden (2014b), DEM simulation of direct shear: 2. Grain boundary and mineral grain strength component influence on shear rupture, *Rock Mech. Rock Eng.*, *47*(5), 1673–1692, doi:10.1007/s00603-013-0494-4.
Blair, S. C., and N. G. W. Cook (1998a), Analysis of compressive fracture in rock using statistical techniques: Part I. A non-linear rule-based model, *Int. J. Rock Mech. Min.*, *35*(7), 837–848, doi:10.1016/S0148-9062(98)00008-4.
Blair, S. C., and N. G. W. Cook (1998b), Analysis of compressive fracture in rock using statistical techniques: Part II. Effect of microscale heterogeneity on macroscopic deformation, *Int. J. Rock Mech. Min.*, *35*(7), 849–861, doi:10.1016/S0148-9062(98)00009-6.
Blake, O. O., and D. R. Faulkner (2016), The effect of fracture density and stress state on the static and dynamic bulk moduli of Westerly granite, *J. Geophys. Res. Solid Earth*, *121*, 2382–2399, doi:10.1002/2015JB012310.
Brace, W. F., B. W. Paulding, and C. Scholz (1966), Dilatancy in the fracture of crystalline rocks, *J. Geophys. Res.*, *71*(16), 3939–3953, doi:10.1029/JZ071i016p03939.
Diederichs, S. M. (2003), Rock fracture and collapse under low confinement conditions, *Rock Mech. Rock Eng.*, *36*(5), 339–381, doi:10.1007/s00603-003-0015-y.
Duan, K., and C. Y. Kwok (2016), Evolution of stress-induced borehole breakout in inherently anisotropic rock: Insights from Discrete Element modeling, *J. Geophys. Res. Solid Earth*, *121*, 2361–2381, doi:10.1002/2015JB012676.
Eberhardt, E., D. Stead, B. Stimpson, and R. Read (1998), Identifying crack initiation and propagation thresholds in brittle rock, *Can. Geotech. J.*, *35*(2), 222–233, doi:10.1139/cgj-35-2-222.
Fakhimi, A., and T. Villegas (2007), Application of dimensional analysis in calibration of a discrete element model for rock deformation and fracture, *Rock Mech. Rock Eng.*, *40*(2), 193–211, doi:10.1007/s00603-006-0095-6.
Fredrich, J. T., B. Evans, and T. F. Wong (1990), Effect of grain size on brittle and semibrittle strength: Implications for micromechanical modelling of failure in compression, *J. Geophys. Res.*, *95*(B7), 10,907–10,920, doi:10.1029/JB095iB07p10907.
Gallagher, J. J., M. Friedman, J. Handin, and G. M. Sowers (1974), Experimental studies relating to microfracture in sandstone, *Tectonophysics*, *21*(3), 203–247, doi:10.1016/0040-1951(74)90053-5.
Geraud, Y., F. Mazerolle, S. Raynaud, and P. Lebon (1998), Crack location in granitic samples submitted to heating, low confining pressure and axial loading, *Geophys. J. Int.*, *133*(3), 553–567, doi:10.1046/j.1365-246X.1998.00471.x.
Güneş Yılmaz, N., R. Mete Goktan, and Y. Kibici (2011), Relations between some quantitative petrographic characteristics and mechanical strength properties of granitic building stones, *Int. J. Rock Mech. Min.*, *48*(3), 506–513, doi:10.1016/j.ijrmms.2010.09.003.
Hadley, K. (1976), Comparison of calculated and observed crack densities and seismic velocities in Westerly granite, *J. Geophys. Res.*, *81*(20), 3484–3494, doi:10.1029/JB081i020p03484.
Hallbauer, D. K., H. Wagner, and N. G. W. Cook (1973), Some observations concerning the microscopic and mechanical behaviour of quartzite specimens in stiff, triaxial compression tests, *Int. J. Rock Mech. Min. Sci. Geomech. Abstr.*, *10*(6), 713–726, doi:10.1016/0148-9062(73)90015-6.
Hofmann, H., T. Babadagli, J. S. Yoon, A. Zang, and G. Zimmermann (2015a), A grain based modeling study of mineralogical factors affecting strength, elastic behavior and micro fracture development during compression tests in granites, *Eng. Fract. Mech.*, *147*, 261–275, doi:10.1016/j.engfracmech.2015.09.008.
Hofmann, H., T. Babadagli, and G. Zimmermann (2015b), A grain based modeling study of fracture branching during compression tests in granites, *Int. J. Rock Mech. Min.*, *77*, 152–162, doi:10.1016/j.ijrmms.2015.04.008.
Ivars, D. M., M. E. Pierce, C. Darcel, J. Reyes-Montes, D. O. Potyondy, R. P. Young, and P. A. Cundall (2011), The synthetic rock mass approach for jointed rock mass modelling, *Int. J. Rock Mech. Min.*, *48*(2), 219–244, doi:10.1016/j.ijrmms.2010.11.014.
Kranz, R. L. (1983), Microcracks in rocks: A review, *Tectonophysics*, *100*(1), 449–480, doi:10.1016/0040-1951(83)90198-1.
Lan, H. X., C. D. Martin, and B. Hu (2010), Effect of heterogeneity of brittle rock on micromechanical extensile behavior during compression loading, *J. Geophys. Res.*, *115*, B01202, doi:10.1029/2009jb006496.
Liu, H. Y., M. Roquete, S. Q. Kou, and P. A. Lindqvist (2004), Characterization of rock heterogeneity and numerical verification, *Eng. Geol.*, *72*(1–2), 89–119, doi:10.1016/j.enggeo.2003.06.004.
Mahabadi, O. K., N. X. Randall, Z. Zong, and G. Grasselli (2012), A novel approach for micro-scale characterization and modeling of geomaterials incorporating actual material heterogeneity, *Geophys. Res. Lett.*, *39*, L01303, doi:10.1029/2011GL050411.
Mahabadi, O. K., B. S. A. Tatone, and G. Grasselli (2014), Influence of microscale heterogeneity and microstructure on the tensile behavior of crystalline rocks, *J. Geophys. Res. Solid Earth*, *119*, 5324–5341, doi:10.1002/2014jb011064.
Manouchehrian, A., and M. Cai (2016), Influence of material heterogeneity on failure intensity in unstable rock failure, *Comput. Geotech.*, *71*, 237–246, doi:10.1016/j.compgeo.2015.10.004.
Martin, C. D., and N. A. Chandler (1994), The progressive fracture of Lac du Bonnet granite, *Int. J. Rock Mech. Min. Sci. Geomech. Abstr.*, *31*(6), 643–659, doi:10.1016/0148-9062(94)90005-1.
Mohsen, N., and C. D. Martin (2014), Factors affecting crack initiation in low porosity crystalline rocks, *Rock Mech. Rock Eng.*, *47*(4), 1165–1181, doi:10.1007/s00603-013-0451-2.
Moore, D. E., and D. A. Lockner (1995), The role of microcracking in shear-fracture propagation in granite, *J. Struct. Geol.*, *17*(1), 95–114, doi:10.1016/0191-8141(94)E0018-T.
Olsson, W. A., and S. S. Peng (1976), Microcrack nucleation in marble, *Int. J. Rock Mech. Min. Sci. Geomech. Abstr.*, *13*(2), 53–59, doi:10.1016/0148-9062(76)90704-X.
Peng, R., Y. Ju, J. G. Wang, H. Xie, F. Gao, and L. Mao (2015), Energy dissipation and release during coal failure under conventional triaxial compression, *Rock Mech. Rock Eng.*, *48*(2), 509–526, doi:10.1007/s00603-014-0602-0.
Peng, S., and A. M. Johnson (1972), Crack growth and faulting in cylindrical specimens of chelmsford granite, *Int. J. Rock Mech. Min. Sci. Geomech. Abstr.*, *9*(1), 37–86, doi:10.1016/0148-9062(72)90050-2.
Potyondy, D. O. (2010), A grain-based model for rock: Approaching the true microstructure, in *Proceedings of the Rock Mechanics in the Nordic Countries*, edited by C. C. Li, pp. 225–234, Norwegian Group for Rock Mechanics, Kongsberg, Norway.
Potyondy, D. O., and P. A. Cundall (2004), A bonded-particle model for rock, *Int. J. Rock Mech. Min.*, *41*(8), 1329–1364, doi:10.1016/j.ijrmms.2004.09.011.
Přikryl, R. (2001), Some microstructural aspects of strength variation in rocks, *Int. J. Rock Mech. Min.*, *38*(5), 671–682, doi:10.1016/S1365-1609(01)00031-4.
Ren, J., and X. Ge (2004), Computerized tomography examination of damage tests on rocks under triaxial compression, *Rock Mech. Rock Eng.*, *37*(1), 83–93, doi:10.1007/s00603-003-0007-y.
Sajid, M., J. Coggan, M. Arif, J. Andersen, and G. Rollinson (2016), Petrographic features as an effective indicator for the variation in strength of granites, *Eng. Geol.*, *202*, 44–54, doi:10.1016/j.enggeo.2016.01.001.
Schlangen, E., and E. J. Garboczi (1997), Fracture simulations of concrete using lattice models: Computational aspects, *Eng. Fract. Mech.*, *57*(2–3), 319–332, doi:10.1016/S0013-7944(97)00010-6.

Schlangen, E., and J. G. M. van Mier (1992), Micromechanics of Failure in Cementitious Composites Experimental and numerical analysis of micromechanisms of fracture of cement-based composites, *Cem. Concr. Compos.*, *14*(2), 105–118, doi:10.1016/0958-9465(92)90004-F.

Sprunt, E. S., and W. F. Brace (1974), Direct observation of microcavities in crystalline rocks, *Int. J. Rock Mech. Min. Sci. Geomech. Abstr.*, *11*(4), 139–150, doi:10.1016/0148-9062(74)92874-5.

Sufian, A., and A. R. Russell (2013), Microstructural pore changes and energy dissipation in Gosford sandstone during pre-failure loading using X-ray CT, *Int. J. Rock Mech. Min.*, *57*, 119–131, doi:10.1016/j.ijrmms.2012.07.021.

Tang, C. A., H. Liu, P. K. K. Lee, Y. Tsui, and L. G. Tham (2000), Numerical studies of the influence of microstructure on rock failure in uniaxial compression—Part I: Effect of heterogeneity, *Int. J. Rock Mech. Min.*, *37*(4), 555–569, doi:10.1016/S1365-1609(99)00121-5.

Tapponnier, P., and W. F. Brace (1976), Development of stress-induced microcracks in Westerly Granite, *Int. J. Rock Mech. Min. Sci. Geomech. Abstr.*, *13*(4), 103–112, doi:10.1016/0148-9062(76)91937-9.

Tuğrul, A., and I. H. Zarif (1999), Correlation of mineralogical and textural characteristics with engineering properties of selected granitic rocks from Turkey, *Eng. Geol.*, *51*(4), 303–317, doi:10.1016/S0013-7952(98)00071-4.

Tullis, J., and R. A. Yund (1977), Experimental deformation of dry westerly granite, *J. Geophys. Res.*, *82*(36), 5705–5718, doi:10.1029/JB082i036p05705.

Weng, M. C., and H. H. Li (2012), Relationship between the deformation characteristics and microscopic properties of sandstone explored by the bonded-particle model, *Int. J. Rock Mech. Min.*, *56*, 34–43, doi:10.1016/j.ijrmms.2012.07.003.

Wong, L. N. Y., and V. Maruvanchery (2016), Different lithological varieties of Bukit Timah Granite in Singapore: A preliminary comparison study on engineering properties, *Rock Mech. Rock Eng.*, *49*(7), 2923–2935, doi:10.1007/s00603-015-0825-8.

Wong, T. F. (1982a), Micromechanics of faulting in westerly granite, *Int. J. Rock Mech. Min. Sci. Geomech. Abstr.*, *19*(2), 49–64, doi:10.1016/0148-9062(82)91631-X.

Wong, T. F. (1982b), Shear fracture of Westerly granite from post failure behavior, *J. Geophys. Res.*, *87*(B2), 990–1000, doi:10.1029/JB087iB02p00990.

Wong, T. F., R. H. C. Wong, K. T. Chau, and C. A. Tang (2006), Microcrack statistics, Weibull distribution and micromechanical modeling of compressive failure in rock, *Mech. Mater.*, *38*(7), 664–681, doi:10.1016/j.mechmat.2005.12.002.

Yang, S. Q., Y. H. Huang, H. W. Jing, and X. R. Liu (2014), Discrete element modeling on fracture coalescence behavior of red sandstone containing two unparallel fissures under uniaxial compression, *Eng. Geol.*, *178*, 28–48, doi:10.1016/j.enggeo.2014.06.005.

Yoon, J. (2007), Application of experimental design and optimization to PFC model calibration in uniaxial compression simulation, *Int. J. Rock Mech. Min.*, *44*(6), 871–889, doi:10.1016/j.ijrmms.2007.01.004.

Zhao, Y., S. Liu, G. F. Zhao, D. Elsworth, Y. Jiang, and J. Han (2014), Failure mechanisms in coal: Dependence on strain rate and microstructure, *J. Geophys. Res. Solid Earth*, *119*, 6924–6935, doi:10.1002/2014JB011198.